

X-ray spectroscopy of the broad line radio galaxy 3C 111

C. S. Reynolds^{1,2}, K. Iwasawa², C. S. Crawford², A. C. Fabian²

¹JILA, University of Colorado, Boulder, CO80309-0440, USA.

²Institute of Astronomy, Madingley Road, Cambridge CB3 0HA.

28 February 2018

ABSTRACT

We present an *ASCA* observation of the broad line radio galaxy 3C 111. The X-ray spectrum is well described by a model consisting of a photoelectrically-absorbed power-law form. The inferred absorbing column density is significantly greater than expected on the basis of 21-cm measurements of Galactic H I. Whilst this may be due intrinsic absorption from a circumnuclear torus or highly warped accretion disk, inhomogeneities and molecular gas within the foreground giant molecular cloud may also be responsible for some of this excess absorption. We also claim a marginal detection of a broad iron $K\alpha$ line which is well explained as being a fluorescent line originating from the central regions of a radiatively-efficient accretion disk. This line appears weak in comparison to those found in (radio-quiet) Seyfert nuclei. We briefly discuss the implications of this fact.

Key words: accretion, accretion discs — galaxies: active — galaxies: individual: 3C 111 — X-rays: galaxies

1 INTRODUCTION

Recent advances in X-ray spectroscopy, currently exemplified by the *ASCA* satellite (Tanaka, Holt & Inoue 1994), have allowed new insights into the astrophysics of the central engines of active galactic nuclei (AGN). Due to their proximity, and comparatively high brightness, the most complete studies have focussed upon Seyfert galaxies. Whereas the underlying emission in Seyfert nuclei over the intrinsic *ASCA* band (0.5–10 keV) is found to be well approximated by a power-law form, most Seyfert nuclei display additional spectral complexity. Substantial photoelectric absorption by cold and/or ionized circumnuclear material is seen in half of all Seyfert 1 nuclei (Fabian et al. 1994; Reynolds 1997) and all Seyfert 2 nuclei. This circumnuclear material may be related to the putative molecular torus, a warped accretion disk, and/or a disk-wind. In addition, almost all Seyfert 1 nuclei are seen to possess a broad, skewed iron $K\alpha$ emission line (Mushotzky et al. 1995; Tanaka et al. 1995; Nandra et al. 1997; Reynolds 1997). This line is thought to be due to fluorescence from the inner regions of the black hole accretion disk that occurs when the disk is strongly irradiated by the X-ray emitting plasma (Tanaka et al. 1995; Fabian et al. 1995). These lines are typically seen to have a full width at half maximum (FWHM) of $100\,000\text{ km s}^{-1}$ and equivalent widths (EW) of 250 eV. A Compton backscattered continuum (the so-called reflection continuum) accompanies these lines at approximately the strength expected on the basis of the X-ray reprocessing model (George & Fabian 1991; Matt, Perola & Piro 1991).

Detailed X-ray spectroscopic studies of radio-loud AGN are rather less complete than that of Seyfert galaxies. This is primarily due to the comparative rarity of radio-loud objects (and, thus, the fact that we have to observe them at greater distance). However, this is a subject of some importance: if the radio-loud/radio-quiet dichotomy reflects fundamental differences in central engine structure, we would expect those differences to be most directly revealed in the X-ray band. The *ASCA* spectrum of the powerful broad line radio galaxy (BLRG) 3C 109 reveals a fairly strong and broad iron line with $\text{FWHM} \sim 120\,000\text{ km s}^{-1}$ and $\text{EW} \sim 300\text{ eV}$ (Allen et al. 1997). This suggests a fundamental similarity between the central engine of this radio galaxy and typical Seyfert nuclei, i.e. that the central parts of the accretion flow are in the form of a geometrically-thin, radiatively-efficient accretion disk. However, 3C 109 might be the exception rather than the rule. Zdziarski et al. (1995) and Woźniak et al. (1997) have shown that BLRGs tend to have slightly weaker iron lines, and appreciably weaker reflection continua, as compared to Seyfert nuclei.

In this paper, we report the results of an *ASCA* observation of 3C 111 ($z = 0.048$). This is an X-ray bright BLRG which is classified as an FR-II source with a double-lobe/single-jet morphology (Linfield & Perley 1984). The inner jet has been seen to display superluminal motion, with apparent outflow velocities of $3.4c$ (Vermeulen & Cohen 1994). Assuming that the pattern speed is intrinsically subluminal, the standard theory of superluminal motion (e.g., see Blandford 1990) implies an upper limit on the angle between the line of sight and the jet axis of $\theta < 32^\circ$.

Section 2 reviews the previous X-ray observations of this source. In Section 3 we describe the basic *ASCA* data analysis and present the results of our spectral fitting. Section 4 discusses the astrophysical implications of our findings. Section 5 draws together our conclusions. We assume that $H_0 = 50 \text{ km s}^{-1} \text{ Mpc}^{-1}$ and $q_0 = 0.5$ throughout this work.

2 A BRIEF X-RAY HISTORY OF 3C 111

3C111 is a well known X-ray source and has been studied by every major X-ray observatory since HEAO 1 A-2. Since it appears as a point X-ray source in every observation made to date, attention has focussed on characterizing its spectral form. To a good approximation, all X-ray spectra of this object are consistent with a power-law spectrum modified by the effects of neutral absorption. Table 1 shows the results of fitting such a model to various historical datasets for 3C 111. Where possible, the data have been retrieved from the High Energy Astrophysics Science Archive Research Center (HEASARC; located at the NASA-Goddard Space Flight Center) and fitted using the appropriate response matrices and background spectra. For completeness, we also report the results of published compilations even for those datasets that we have re-analyzed.

Comparing the detailed fits of these different instruments is wrought with the dangers of cross-calibration uncertainties. We do not attempt any such comparison here and simply present Table 1 for completeness and illustration. However, we note one particularly interesting feature. The *EXOSAT* medium energy array (ME) observed 3C 111 on two occasions separated by almost two and a half months. It is evident from both the fits in Table 1 and a visual examination of the two spectra that significant spectral variability occurs between these two periods. In particular, the absorption column is seen to dramatically increase from being less than $6.6 \times 10^{21} \text{ cm}^{-2}$ to greater than $3.42 \times 10^{22} \text{ cm}^{-2}$. Since this significant change is seen in two spectra from the same instrument, it appears to be a robust result. We briefly discuss the possible physical nature of this change in Section 4.

3 ANALYSIS OF THE *ASCA* DATA

3.1 Basic data reduction

The *ASCA* observation of 3C 111 was performed on 1996 February 13/14 with a total duration of approximately one day. Data were collected from both the Solid-state Imaging Spectrometers (SIS) and Gas Imaging Spectrometers (GIS). The two SIS detectors were used in 1-CCD mode due to telemetry constraints. After applying standard data cleaning and selection criteria (explicitly defined in Reynolds 1997), there was a total of 32 800 s of useful SIS data, and 38 000 s of useful GIS data. These shall be referred to as ‘good’ data. Table 2 summarizes the basic parameters of this observation.

There is no evidence for spatial extent beyond that of the point spread function in any of the images resulting from the four detectors. Lightcurves and spectra were extracted using circular regions centred on the centroid of the source counts. We used an extraction radius of 3 arcmins for the SIS

parameter	value
obs. date	13/14-Feb-1996
good SIS time	32 800 s
good GIS time	38 000 s
SIS0 count rate	0.702 ct s^{-1}
GIS2 count rate	0.542 ct s^{-1}
0.5–2 keV flux	$5.0 \times 10^{-12} \text{ erg cm}^{-2} \text{ s}^{-1}$
2–10 keV flux	$3.5 \times 10^{-11} \text{ erg cm}^{-2} \text{ s}^{-1}$
0.5–2 keV luminosity	$2.2 \times 10^{44} \text{ erg s}^{-1}$
2–10 keV luminosity	$3.9 \times 10^{44} \text{ erg s}^{-1}$

Table 2. Basic parameters of the *ASCA* observation of 3C 111. The quoted fluxes are those observed (i.e. subject to the total line of sight absorption), but the quoted luminosities are the intrinsic (i.e. un-absorbed) values. Spectral model-E of Table 3 was used to determine the flux and luminosity.

data, and 4 arcmins for the GIS data. These regions are sufficiently large to contain all but a small portion of the source counts. Background spectra were extracted from source free regions of the same fields for each of the four detectors. Background regions for the SIS were taken to be rectangular regions along the edges of the source chip, whereas annular regions were used for GIS background. Following standard practices, our spectra were rebinned such as to contain at least 20 photons per spectral bin. This ensures that the photon number in each spectral bin is approximately described by a normal distribution, a necessary condition for χ^2 analysis to be valid. Table 2 reports the resulting (background subtracted) count rates, fluxes and inferred luminosities.

The light curves from each detector were examined for variability. No evidence for variability was found, i.e., χ^2 analysis found that a constant X-ray flux is completely consistent with the *ASCA* lightcurves.

3.2 Spectral analysis

In the absence of any spatial or temporal structure, we shall concentrate on an analysis of the spectrum. In order to avoid poorly calibrated regions of the spectrum, we limited the SIS analysis to the 0.55–10 keV band, and GIS analysis to the 1–10 keV band. For convenience, the results of the following analysis are summarized in Table 3.

Narrow beam 21-cm measurements suggest that the Galactic H I column density towards 3C 111 is $N_{\text{H}}(\text{Gal}) = 3.26 \times 10^{21} \text{ cm}^{-2}$ (Elvis, Lockman & Wilkes 1989). However, it must be noted that 3C 111 lies behind a well-known Galactic molecular cloud. Inhomogeneities within this cloud on a scale smaller than that probed by the 21-cm measurements might lead to differences between the real Galactic column density towards the X-ray source in 3C 111, and that suggested by the H I measurements. Furthermore, molecular regions will contribute to the X-ray opacity but not to the 21-cm flux. We shall return to this issue in Section 4.

3.2.1 Basic spectral form and characterization of the X-ray absorption

All spectral analysis reported in this paper is based upon joint fitting of the SIS and GIS data. The normalizations

Observatory & Instrument	Observation Date	Photon Index	Absorbing column (10^{20} cm^{-2})	2-10 keV Flux ($10^{-11} \text{ erg cm}^{-2} \text{ s}^{-1}$)	Reference
HEAO 1	1978-Sep-3	$1.89^{+0.18}_{-0.17}$	194^{+101}_{-94}	3.9	Weaver et al. (1995)
Einstein SSS	1979-Mar-2	$1.47^{+0.47}_{-0.38}$	40^{+38}_{-26}	unconstrained	HEASARC
Einstein MPC	1979-Mar-2	$1.56^{+0.50}_{-0.68}$	< 252	4.3	HEASARC
Einstein SSS/MPC	1979-Mar-2	$1.44^{+0.22}_{-0.20}$	36^{+29}_{-7}	4.2	Turner et al. (1991)
EXOSAT ME	1983-Nov-14	$1.35^{+0.31}_{-0.22}$	< 66	1.63	HEASARC
EXOSAT ME	1984-Jan-27	$2.71^{+1.50}_{-1.10}$	815^{+726}_{-473}	0.97	HEASARC
EXOSAT LE/ME	1984-Jan-27	$1.4^{+0.9}_{-0.7}$	80^{+250}_{-50}	1.8	Turner & Pounds (1989)
Ginga LAC	1989-Feb-4	$1.77^{+0.04}_{-0.03}$	181^{+18}_{-13}	3.1	Nandra & Pounds (1994)
ROSAT PSPC(B)	1990-Jun-1	$1.49^{+1.42}_{-1.20}$	67^{+39}_{-31}	unconstrained	HEASARC
ASCA SIS/GIS	1996-Feb-13	$1.72^{+0.09}_{-0.04}$	95^{+5}_{-4}	3.5	this work

Table 1. The X-ray history of 3C 111 including the current work. Shown here are the results of fitting a simple absorbed power-law form to the relevant data. Those datasets referenced as HEASARC have been retrieved from the HEASARC database and fitted with an absorbed power-law model. The errors are quoted at the 90 per cent level for one interesting parameters ($\Delta\chi^2 = 2.71$).

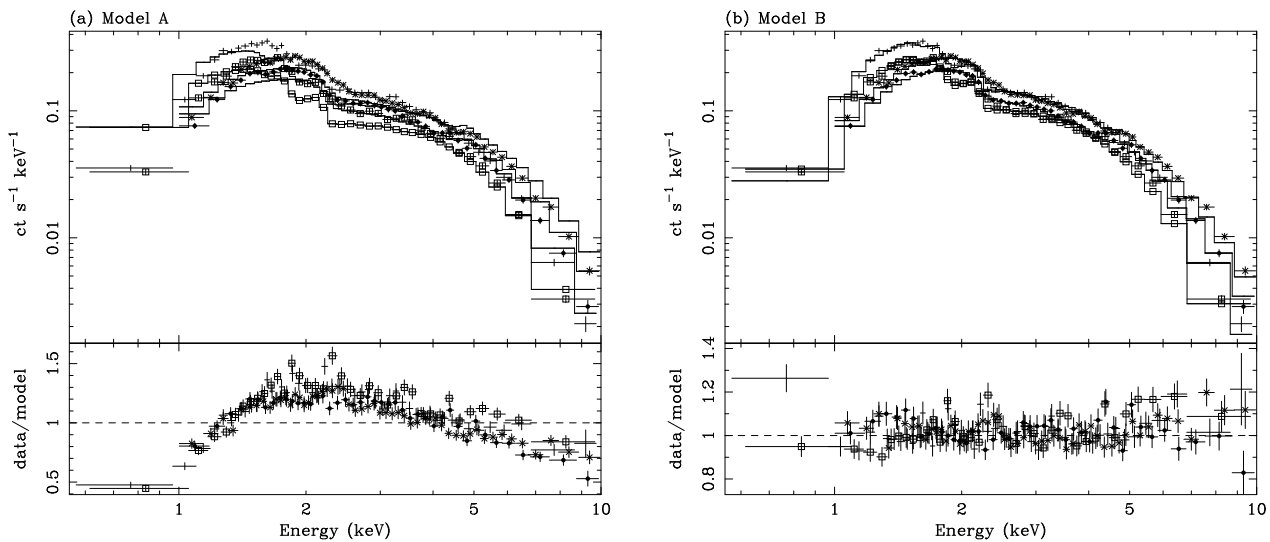


Figure 1. ASCA spectrum of 3C 111. Panel (a) shows the data fitted to a power-law form modified only by Galactic absorption at the level suggested by HI 21-cm measurements (model A in Table 3). Note the clear deficit of counts at soft energies indicating the need for extra absorption. Panel (b) shows the data fitted with a model consisting of a power-law form modified by absorption due to a $z = 0$ neutral absorber (model B in Table 3). The data from all four instruments are shown: SIS0 (plain crosses), SIS1 (open squares), GIS2 (filled circles) and GIS3 (diagonal crosses). For clarity of presentation, the spectral bins have been re-grouped by a factor of 20.

of the model for each of the four instruments were left as free parameters to allow for the ~ 10 per cent uncertainties in the overall flux calibration of the different instruments. However, we have noted a slight discrepancy between the SIS and GIS data. When taken alone, the SIS data present marginal evidence for a spectral break at 4 keV with photon indices $\Gamma \approx 1.9$ below the break and $\Gamma \approx 1.6$ above the break ($\Delta\chi^2 = 11$ for two additional degrees of freedom as compared with the unbroken power-law). However, this break is *not* required when the GIS data are also considered. Furthermore, the GIS data taken alone show no evidence for an iron emission line whereas the SIS data do show marginal evidence. Given the marginal nature of these differences, and the remaining calibration uncertainties present in the current analysis tools, we have chosen to take the conservative approach and deal only with the joint SIS/GIS spectrum.

Initially, we fitted the joint spectrum with a power-law form modified only by Galactic absorption at the level indicated by the 21-cm measurements. As can be seen from

Table 3, this fit is a dreadful description of the data, yielding a goodness of fit parameter $\chi^2/\text{dof}=5293/1725$. Inspection of the residuals clearly indicates the need for absorption in excess of that indicated by the 21-cm measurements (see Fig. 1a). Thus, we consider additional column densities of neutral absorbing material placed either in our Galaxy (i.e. $z = 0$) or at 3C 111 (i.e. $z = 0.048$). Both of these cases provided a statistically satisfactory description of the overall spectrum, with required addition column densities of $N_{\text{H}} = (6.2^{+0.3}_{-0.2}) \times 10^{21} \text{ cm}^{-2}$ and $N_{\text{H}} = (7.0^{+0.2}_{-0.3}) \times 10^{21} \text{ cm}^{-2}$ for the $z = 0$ and $z = 0.048$ absorbers respectively. Figure 1b shows the spectral fit for the case of the $z = 0$ absorber (although a very similar fit results for the $z = 0.048$ absorber).

Inspection of Fig. 1 shows that the SIS0 data argue for extra soft emission beyond that predicted by the model. However, this conclusion is not supported by data from SIS1. Furthermore, examination of GIS2/GIS3 data below 1 keV (not shown on Fig. 1) also fails to provide any evidence for a ‘soft excess’. The level of this soft feature is much greater

model	model specifications	parameter values	χ^2/dof
A	NH(Gal)+PL	$N_{\text{H}}(\text{Gal}) = 3.26 \times 10^{21} \text{ cm}^{-2}$ (fixed) $\Gamma = 1.13 \pm 0.01$	5293/1725
B	NH(Gal)+NH+PL	$N_{\text{H}}(\text{Gal}) = 3.26 \times 10^{21} \text{ cm}^{-2}$ (fixed) $N_{\text{H}} = (6.2^{+0.3}_{-0.2}) \times 10^{21} \text{ cm}^{-2}$ $\Gamma = 1.72^{+0.03}_{-0.02}$	1653/1724
C	NH(Gal)+zNH+PL	$N_{\text{H}}(\text{Gal}) = 3.26 \times 10^{21} \text{ cm}^{-2}$ (fixed) $N_{\text{H}} = (7.0^{+0.2}_{-0.3}) \times 10^{21} \text{ cm}^{-2}$ $\Gamma = 1.72 \pm 0.02$	1659/1724
D	NH(Gal)+WARM+PL	$N_{\text{H}}(\text{Gal}) = 3.26 \times 10^{21} \text{ cm}^{-2}$ (fixed) $N_{\text{W}} = (7.9^{+0.6}_{-1.2}) \times 10^{21} \text{ cm}^{-2}$ $\xi < 7.3 \text{ erg s}^{-1} \text{ cm}$ $\Gamma = 1.65^{+0.03}_{-0.04}$	1660/1723
E	NH(Gal)+NH+PL+nGAU	$N_{\text{H}}(\text{Gal}) = 3.26 \times 10^{21} \text{ cm}^{-2}$ (fixed) $N_{\text{H}} = (6.3^{+0.3}_{-0.2}) \times 10^{21} \text{ cm}^{-2}$ $\Gamma = 1.73 \pm 0.02$ $E = 6.4 \pm 0.2 \text{ keV}$ $W = 20^{+25}_{-16} \text{ eV}$	1649/1722
F	NH(Gal)+NH+PL+bGAU	$N_{\text{H}}(\text{Gal}) = 3.26 \times 10^{21} \text{ cm}^{-2}$ (fixed) $N_{\text{H}} = (6.4 \pm 0.3) \times 10^{21} \text{ cm}^{-2}$ $\Gamma = 1.75 \pm 0.03$ $E = 6.2^{+1.8}_{-0.9} \text{ keV}$ $\sigma = 0.6^{+\infty}_{-0.5} \text{ keV}$ $W > 20 \text{ eV}$	1644/1721
G	NH(Gal)+NH+PL+DISK	$N_{\text{H}}(\text{Gal}) = 3.26 \times 10^{21} \text{ cm}^{-2}$ (fixed) $N_{\text{H}} = (6.4 \pm 0.3) \times 10^{21} \text{ cm}^{-2}$ $\Gamma = 1.75 \pm 0.03$ $r_{\text{in}} = 6r_{\text{g}}$ (fixed) $r_{\text{out}} = 1000r_{\text{g}}$ (fixed) $i < 32^\circ$ $\beta < -2.2$ $W = 100^{+95}_{-60} \text{ eV}$	1643/1721
H	NH(Gal)+NH+PL+DISK	$N_{\text{H}}(\text{Gal}) = 3.26 \times 10^{21} \text{ cm}^{-2}$ (fixed) $N_{\text{H}} = (6.4 \pm 0.3) \times 10^{21} \text{ cm}^{-2}$ $\Gamma = 1.75 \pm 0.03$ $r_{\text{in}} < 18r_{\text{g}}$ $r_{\text{out}} = 1000r_{\text{g}}$ (fixed) $i < 32^\circ$ $\beta = -3$ (fixed) $W = 110^{+60}_{-70} \text{ eV}$	1643/1721

Table 3. Spectral fitting results for 3C 111. Model abbreviations follow: NH(Gal) = Galactic column density as inferred from H I measurements, NH = additional (neutral) Galactic column density (column N_{H}), zNH = additional (neutral) column density located at 3C 111 (column N_{H}), WARM = ionized (warm) absorber (column N_{W} , ionization parameter ξ ; see Section 3.2.1), PL = power-law emission (photon index Γ), nGAU = narrow Gaussian emission line (centroid energy E and equivalent width W), bGAU = broad Gaussian emission line (centroid energy E , standard deviation σ and equivalent width W). DISK = diskline model (see Section 3.2.2 of main text for description). All errors are quoted at the 90 per cent confidence level for one interesting parameter, $\Delta\chi^2 = 2.7$.

than the SIS0 background level at those energies, and so we rule out the possibility that poor background subtraction is responsible for this contradiction. We must conclude that this soft feature seen in SIS0 is not physical and results from an extreme statistical fluctuation or some currently unrecognized instrumental anomaly.

For completeness, we have also examined the possibility of absorption by partially photoionized line-of-sight gas. Such absorption is commonly seen in the soft X-ray spectrum of Seyfert 1 galaxies where it is often referred to as

‘warm’ absorption. We have constructed a photoionization model of an incident power-law spectrum passing through a slab of gas with total column density N_{W} and ionization parameter ξ . This ionization parameter is defined by

$$\xi = \frac{L_{\text{i}}}{n_{\text{e}} r^2}, \quad (1)$$

where L_{i} is the ionizing luminosity (i.e. the luminosity in photons above 13.6 eV), n_{e} is the electron number density of the gas, and r is the distance of the gas from the ioniz-

ing source. For detailed of this photoionization model, see Reynolds (1997) For a wide range of parameter space, the ionization state of the gas, and hence its X-ray opacity, depends only on ξ . This is presented as model-D in Table 3.

From table 3 it can be seen that the data do not require an ionized absorber as is apparent from the fact that we can only impose an upper limit on the ionization parameter $\xi < 7.3 \text{ erg cm s}^{-1}$. Note that even this upper limit is significantly below the typical values found in Seyfert galaxies, $\xi \sim 20 \text{ erg cm s}^{-1}$.

3.2.2 The iron line

The $K\alpha$ iron emission line is of some importance since it probes structures deep within the central engine. Here, we examine the 3C 111 data for evidence of such a line.

Throughout this section, we take the simple absorbed power-law model (model B in Table 3) as our base model. To this base model, we added a narrow Gaussian feature at $E = 6.4 \text{ keV}$ (in the rest frame of 3C 111) and performed a χ^2 minimization (leaving the energy E and normalization of the line as free parameters, but constraining the line to be narrow). The results are given in Table 3 (model E). The improvement in the goodness of fit, $\Delta\chi^2 = 4.3$ is *not* significant at the 90 per cent level according to the F-test for two extra degrees of freedom. However, we obtain a stronger result if we add a broad Gaussian line to model B (reported as model F in Table 3): the improvement in the goodness of fit parameter, $\Delta\chi^2 = 9$, is significant at the 90 per cent level, but not at the 95 per cent level. Thus, we claim a marginal detection of a broad iron line. However, due to the marginality of the detection, the best fitting parameters of the broad Gaussian are very poorly constrained, as can be seen by inspection of Table 3.

To make further progress, we assume that this line arises by the fluorescence of ‘cold’* iron in an accretion disk around a Schwarzschild black hole. The expected line profiles for this case have been calculated by Fabian et al. (1989) and are incorporated into the spectral fitting package XSPEC as the ‘diskline’ model.

We considered two cases. In the first case (model G), the inner radius of the line emitting region was fixed to correspond to the radius of marginal stability $r_{\text{in}} = 6r_{\text{g}}$, where r_{g} is the gravitational radius of the black hole. The outer radius of the line emitting region was fixed at $r_{\text{out}} = 1000r_{\text{g}}$. We can justify fixing this parameter since the line profile is insensitive to r_{out} provided that $r_{\text{out}} \gg r_{\text{in}}$ and the line emissivity declines with radius in the disk faster than r^{-2} . We make the canonical simplification that the line emissivity depends on the radius in a power-law sense, $\epsilon \propto r^\beta$, where β is left as a free parameter in the fit. The inclination of the disk, i , and normalization of the line were also left as free parameters in the fit. Our second case (model H) is similar except that we fix the emissivity index to be $\beta = -3$ and allow the inner radius of the line emitting region to be a free parameter. This line emissivity law ($\beta = -3$) is the asymptotic behaviour for large r in the case where the primary X-ray source is either a point X-ray source on the symmetry

axis of the disk, or is a thin corona with a local power that tracks the viscous dissipation in the underlying disk (Page & Thorne 1974).

The results of spectral fitting with models G and H are shown in Table 3. Several of these results are noteworthy. First, both models imply a disk inclination of $i < 32^\circ$, completely consistent with the limits on the angle between the line of sight and the jet axis imposed by observations of the superluminal motion (see Introduction). Secondly, interesting constraints can be placed on the equivalent width of the iron line, $W = 40 - 195 \text{ eV}$ (90 per cent bounds). This contrasts with the broad Gaussian parameterization, with which only a lower limit on W could be obtained. The reason for this is easily seen. The broad Gaussian fit is subject to a statistical instability in which both the width and equivalent width of the Gaussian grow arbitrary large. In other words, the Gaussian component can mimic the high-energy region of the continuum making meaningful constraints on the EW of the line impossible. However, the disk-line model imposes a physical limit on the maximum width of the iron line, thereby allowing the equivalent width to be usefully constrained. Thirdly, model H shows that the line emitting region must extend at least down to within $18r_{\text{g}}$ of the black hole.

4 DISCUSSION

These *ASCA* data confirm the need for a substantial amount of absorption beyond that expected on the basis of 21-cm Galactic H I measurements. However, these data cannot distinguish between an absorber which is intrinsic to the 3C 111 system (i.e., at $z = 0.048$) or one that is more local to us. The small difference in the goodness of fit between model B (i.e. the local absorber) and model C (i.e., the absorber at $z = 0.048$) may be influenced by the small soft excess seen in the SIS0 data. Since we presume this soft excess to be spurious (Section 3.2.1), we must treat model B and model C as providing similarly good fits to these data.

Given this freedom in the spectral data, there are at least three possibilities for the nature of this absorber. First, the excess absorbing material may be the neutral component of the ISM of the 3C 111 host galaxy. Given the large column of material required (almost 10^{22} cm^{-2}), this would suggest that the host galaxy was a disk galaxy viewed at high inclination. This is inconsistent with the apparent cD nature of the host galaxy (Owen & Laing 1989). Thus, we argue against this possibility.

Secondly, the excess absorbing material maybe circumnuclear material associated directly with the AGN (e.g., the putative molecular torus of AGN unification schemes or the outer parts of a warped accretion disk.) Observations of the iron line and, independently, superluminal motion imply a central engine inclination of $i < 32^\circ$ (i.e., we are viewing the central engine somewhat face-on). Within the ‘‘circumnuclear absorber’’ picture, we would be led to the conclusion that a relatively large quantity of neutral material must exist at high latitudes within the system. This would suggest a molecular torus with a small opening angle or a highly warped accretion disk.

In most cases, X-ray absorption towards an AGN in excess of that suggested by Galactic H I measurements is taken

* By ‘cold’, we mean in the ionization range Fe I–Fe XVII, giving a rest frame line energy of 6.4 keV.

to be firm evidence for intrinsic absorption associated with either the AGN or its host galaxy. Whilst the absorbing material seen towards 3C 111 may indeed be circumnuclear in nature, we might question this inference given the fact that 3C 111 lies behind a well known giant molecular cloud (containing Taurus B and the Taurus-Perseus complexes) estimated to lie at a distance of 350 pc (Ungerechts & Thaddeus 1987). There are two ways in which the presence of this cloud complex can cause deviations between the actual Galactic absorption along the line of sight and that inferred from 21-cm measurements: small scale inhomogeneities and the presence of molecular hydrogen. We note that Turner et al. (1995) made a similar suggestion for the case of NRAO 140.

Marscher, Moore & Bania (1993) and Moore & Marscher (1995) have used 3C 111 as a background radio continuum source to probe details of the 4.83 GHz H_2CO absorption line arising from material in this molecular cloud. On the basis of temporal variability in the strength and profile of the absorption line, they argue that the cloud complex contains inhomogeneities on the sub-parsec, or even AU, scales[†]. These authors estimate that between 30–100 clumps lie along the line-of-sight to 3C 111 and that Poisson fluctuations in this number give rise to the observed molecular line changes. The 21-cm studies of Elvis, Lockman & Wilkes (1989) use a 21×21 arcmin² beam (Lockman, Jahoda & McCammon 1986) – measurements of the neutral hydrogen column densities are necessarily averaged over this beam and hence insensitive to the small scale inhomogeneities indicated by the molecular absorption line studies. Thus, these inhomogeneities could give rise to differences between the 21-cm column density and observed absorbing column. However, given that 3C 111 appears *not* to be blocked by one (or a small number) especially dense clump, it is difficult to envisage the factor of 3 discrepancy between the 21-cm measurements and X-ray absorption as arising purely from these inhomogeneities.

Clearly, we expect there to be molecular hydrogen along our line of sight to 3C 111 associated with the molecular cloud. This gas, and the metals/dust associated with it, will act as a source of X-ray opacity which is indistinguishable from atomic gas at the spectral resolution of *ASCA*. Since it does not contribute to the 21-cm emission, this molecular gas is another possible cause for the discrepancy between the 21-cm measurements and the X-ray absorbing column. If 60–70 per cent of the gas along the line of sight to 3C 111 is in molecular form, the discrepancy between the 21-cm measurements and the X-ray absorbing column is resolved. Furthermore, the clear temporal change in absorption between the two *EXOSAT* ME spectra discussed in Section 2 might be due to a particularly large inhomogeneity/knot in this molecular gas that drifts across the line of sight to the core of 3C 111.

We also claim the marginal detection of a broad iron line. Although the constraints are poor, the data are consistent with a cold iron line originating from the central regions of an accretion disk around a Schwarzschild black

hole. The disk inclination is constrained to be $i < 32^\circ$. The equivalent width, $W = 40 - 195$ eV, is rather weak as compared to Seyfert nuclei (Nandra et al. 1997; Reynolds 1997). This is consistent with the results of Woźniak et al. (1997) who examine *OSSE/Ginga* data and find an iron line EW of ~ 70 eV and a weak reflection continuum. This authors find that the inferred solid angle subtended by the ‘reflector’ at the X-ray source is $\Omega/2\pi \sim 0.3$. As mentioned in the Introduction, this is found to be a general trend differentiating radio-quiet Seyfert nuclei from BLRGs.

These iron line studies suggest both fundamental similarities and differences between the central engines of radio-quiet Seyfert nuclei and BLRGs. The fact that BLRGs display resolved iron lines at all is evidence for the existence of a geometrically-thin, radiatively efficient accretion disk extending down to $r \lesssim 20r_g$, as is the case for Seyfert nuclei (note that in the Seyfert case, iron line studies seem to suggest that the disk remains geometrically-thin and radiatively-efficient essentially all of the way down to the black hole). The comparative weakness of the lines/reflection-continua in BLRG could arise for several reasons. First, there might be a component of the X-ray emission that is associated with the radio jet and is beamed along the jet axis thereby diluting the Seyfert-like reflection features that are intrinsically present. Secondly, the inner accretion disk (i.e. the inner $20r_g$ or so) might not be in a physical state capable of producing the X-ray reflection features. For example, the disk might undergo a transition into an optically-thin advection dominated disk (ADD) which would be totally ionized and hence incapable of producing X-ray reflection signatures. If most of the primary X-ray flux still originated from the central most regions, the solid angle covered by material capable of producing reflection features could be rather small. Such models (with a thin-disk/ADD transition) have previously been discussed in the context of Galactic Black Hole Candidates (e.g., see Esin, McClintock & Narayan 1997 and references therein).

5 CONCLUSIONS

Our *ASCA* data for 3C 111 clearly reveal the presence of absorption in excess to that suggested by 21-cm measurements of the Galactic H I column. Whilst this may be evidence for absorption intrinsic to the 3C 111 system, we suggest that inhomogeneities and molecular material in the foreground (Galactic) giant molecular cloud may also be responsible for this excess absorption. Molecular absorption line studies of this cloud lend strength to this possibility.

We also claim the marginal detection of a broad iron $K\alpha$ line. The detection of a broad line at all suggests the existence of a geometrically-thin, radiatively-efficient accretion disk within $r \lesssim 20GM/c^2$ of the black hole. However, the weakness of this line (and the associated backscattered continuum) as compared to typical Seyfert galaxies suggests that either X-ray beaming is important, or that the innermost regions of the disk are in a state incapable of producing the X-ray reflection signatures. One possibility is that the disk undergoes a transition to an ADD state in its innermost regions.

[†] We note that Thoraval, Boisse & Stark (1996) dispute the existence of AU scale inhomogeneities in this cloud based on the apparent lack of reddening variability in a sample of stars in this field.

ACKNOWLEDGMENTS

We acknowledge support from PPARC (CSR, CSC, KI), the Royal Society (ACF), the National Science Foundation under grant AST9529175 (CSR), and NASA under grant NASA-NAG5-6337 (CSR).

REFERENCES

- Allen S. W., Fabian A. C., Idesawa E., Inoue H., Kii T., Otani C., 1997, MNRAS, 286, 765
- Blandford R. D., 1990, in Active Galactic Nuclei, ed T.J.-L. Courvoisier & M. Mayor (Saas-Fee Advanced Course 20) (Berlin:Springer), p.161
- Elvis M., Lockman F. J., Wilkes B. J., 1989, AJ, 97, 777
- Esin A. A., McClintock J. E., Narayan R., 1997, ApJ, submitted
- Fabian A. C., Rees M. J., Stellar L., White N. E., 1989, MNRAS, 238, 729
- Fabian A. C. et al. 1994, PASJ, 46, L59
- Fabian A. C. et al. 1995, MNRAS, 277, L11
- George I. M., Fabian A. C., 1991, MNRAS, 249, 352
- Linfield R., Perley R., 1984, ApJ, 279, 60
- Lockman F. J., Jahoda K., McCammon D., 1986, ApJ, 302, 432
- Marscher A. P., Moore E. M., Bania T. M., 1993, ApJ, 419, L101
- Matt G., Perola G. C., Piro L., 1991, A&A, 247, 25
- Moore E. M., Marscher A. P., 1995, ApJ, 452, 671
- Mushotzky R. F., Fabian A. C., Iwasawa K., Kunieda H., Matsuoka M., Nandra K., Tanaka Y., 1995, MNRAS, 272, L9
- Nandra K., Pounds K. A., 1994, MNRAS, 268, 405
- Nandra K., George I. M., Mushotzky R. F., Turner T. J., Yaqoob T., 1997, ApJ, 477, 602
- Owen F. N., Laing R. A., 1989, MNRAS, 238, 357
- Page D. N., Thorne K. S., 1974, ApJ, 499, 191
- Reynolds C. S., 1997, MNRAS, 286, 513
- Tanaka Y., Inoue H., Holt S. S., 1994, PASJ, 46, L37
- Tanaka Y. et al., 1995, Nat, 375, 659
- Thoraval S., Boisse P., Stark R., 1996, A&A, 312, 973
- Turner T. J., Pounds K. A., 1989, MNRAS, 240, 833
- Turner T. J., Weaver K. A., Mushotzky R. F., Holt S. S., Madejski G. M., 1991, ApJ, 381, 85
- Turner T. J., George I. M., Madejski G. M., Kitamoto S., Suzuki T., 1995, ApJ, 445, 660
- Ungerechts H., Thaddeus P., 1987, ApJS, 63, 645
- Vermeulen R. C., Cohen M. H., 1994, ApJ, 430, 467
- Weaver K. A., Arnaud K. A., Mushotzky R. F., 1995, ApJ, 447, 121
- Woźniak P. R., Zdziarski A. A., Smith D., Madejski G. M., Johnson W. N., 1997, MNRAS, submitted
- Zdziarski A. A., Johnson W. N., Done C., Smith D., McNaron-Brown K., 1995, ApJ, 438, L63